

Quantum phase transition triggering magnetic BICs in graphene

L. H. Guessi¹, Y. Marques², R. S. Machado², K. Kristinsson³,

L. S. Ricco², I. A. Shelykh^{3,4,5}, M. S. Figueira⁶, M. de Souza^{1,*} and A. C. Seridonio^{1,2}

¹IGCE, Unesp - Univ Estadual Paulista, Departamento de Física, 13506-900, Rio Claro, SP, Brazil

²Departamento de Física e Química, Unesp - Univ Estadual Paulista, 15385-000, Ilha Solteira, SP, Brazil

³Division of Physics and Applied Physics, Nanyang Technological University 637371, Singapore

⁴Science Institute, University of Iceland, Dunhagi-3, IS-107, Reykjavik, Iceland

⁵ITMO University, St. Petersburg 197101, Russia

⁶Instituto de Física, Universidade Federal Fluminense, 24210-340, Niterói, RJ, Brazil

Graphene hosting a pair of collinear adatoms in the phantom atom configuration has density of states vanishing in the vicinity of the Dirac point which can be described in terms of the pseudogap scaling as cube of the energy, $\Delta \propto |\varepsilon|^3$ which leads to the appearance of spin-degenerate bound states in the continuum (BICs) [Phys. Rev. B **92**, 045409 (2015)]. In the case when adatoms are locally coupled to a single carbon atom the pseudogap scales linearly with energy, which prevents the formation of BICs. Here, we explore the effects of non-local coupling characterized by the Fano factor of interference q_0 , tunable by changing the slope of the Dirac cones in the graphene band-structure. We demonstrate that three distinct regimes can be identified: i) for $q_0 < q_{c1}$ (critical point) a mixed pseudogap $\Delta \propto |\varepsilon|, |\varepsilon|^2$ appears yielding a phase with spin-degenerate BICs; ii) near $q_0 = q_{c1}$ when $\Delta \propto |\varepsilon|^2$ the system undergoes a quantum phase transition (QPT) in which the new phase is characterized by magnetic BICs and iii) at a second critical value $q_0 > q_{c2}$ the cubic scaling of the pseudogap with energy $\Delta \propto |\varepsilon|^3$ characteristic to the phantom atom configuration is restored and the phase with non-magnetic BICs is recovered. The phase with magnetic BICs can be described in terms of an effective intrinsic exchange field of ferromagnetic nature between the adatoms mediated by graphene monolayer. We thus propose a new type of QPT resulting from the competition between two ground states, respectively characterized by spin-degenerate and magnetic BICs.

PACS numbers: 72.80.Vp, 07.79.Cz, 72.10.Fk

I. INTRODUCTION

Graphene-based systems are promising candidates for the detection of the so-called bound states in the continuum (BICs)^{1,2}. BICs were first theoretically predicted by von Neumann and Wigner in 1929³ as quantum states with localized square-integrable wave functions, but having energies within the continuum of delocalized states. The electrons within BICs do not decay into the system continuum, thus these states should be invisible in transport experiments.

The subject experienced revival after the work of Stillinger and Herrick in 1975⁴. Since then, BICs were predicted to appear in a variety of electronic, optical and photonic systems^{1,5,6}. In these systems, effects of Fano interference⁷ were proposed as the underlying mechanism for the emergence of BICs and their possible experimental observation. In particular, we recently proposed that BICs can be observed in the system of graphene with two collinear adatoms in the phantom atom configuration¹.

In this work, we show that the setup outlined in Fig.1 for suspended graphene can undergo a quantum phase transition (QPT) into the state with magnetic BICs if non-local graphene-adatom couplings are taken into account. The phenomenon is a consequence of the particular scaling of the local density of states (LDOS) \mathcal{D}_0 on energy ε in the vicinity of the Dirac point. The latter is proportional to the quantity known as *pseudogap* Δ , related to the intensity of the scattering near the Fermi

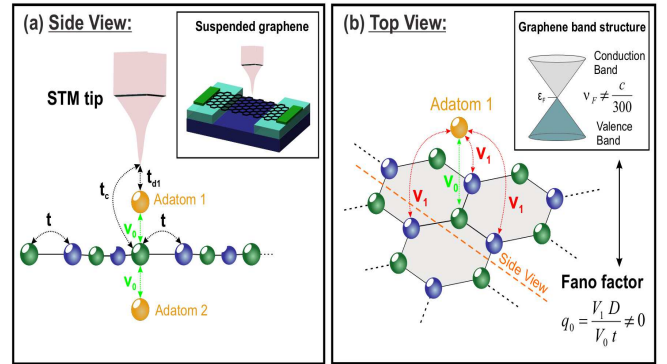


Figure 1. (Color online) (a) Side view: two adatoms labeled by 1 (upper) and 2 (lower) placed collinear to a carbon atom beneath an STM tip in suspended graphene (inset) (b) Top view: the adatoms are coupled to the carbon atom beneath them and its nearest neighbors. The relative strength of these couplings define the Fano factor of interference q_0 playing the role of the natural control parameter of the system. It can be tuned by varying the slope of the Dirac cones in the graphene band-structure (inset).

energy^{8,9}. Formation of the magnetic BICs becomes possible only if $\Delta \propto |\varepsilon|^2$ similar to the transition reported in Ref. [8] for a pair of quantum dots coupled to metallic leads.

The QPT reported here is driven by a Fano factor

of interference q_0 which can be thus considered as the natural control parameter of the system. It can be tuned by changing the slope of the Dirac cones in the graphene band-structure (see Fig.1(b)). The magnetic BICs appear within the region inside the critical boundaries $q_{c1} < q_0 < q_{c2}$, where the dominant scaling law for the pseudogap is quadratic ($\Delta \propto |\varepsilon|^2$). Outside this region, the mixed scaling $\Delta \propto |\varepsilon|, |\varepsilon|^2$ for $q_0 < q_{c1}$ or cubic scaling $\Delta \propto |\varepsilon|^3$ for $q_0 > q_{c2}$, leads to the formation of spin-degenerate BICs. The transition towards the magnetic BIC state is triggered due to the onset of the effective intrinsic ferromagnetic exchange field $\mathcal{J}^{\text{exch}}$ between the adatoms mediated by the graphene monolayer.

II. THE MODEL

To give a theoretical description of the setup plotted in Fig.1, we use the model based on the Anderson Hamiltonian^{10,11}:

$$\begin{aligned} \mathcal{H}_{2D} = & \sum_{s\sigma} \int dk (\hbar v_F k) c_{sk\sigma}^\dagger c_{sk\sigma} + \sum_{j\sigma} \varepsilon_{jd} d_{j\sigma}^\dagger d_{j\sigma} \\ & + \mathcal{U} \sum_j n_{d_j\uparrow} n_{d_j\downarrow} + \sum_{js\sigma} \int dk \mathcal{V}_k (c_{sk\sigma}^\dagger d_{j\sigma} + \text{H.c.}), \end{aligned} \quad (1)$$

with v_F being Fermi velocity. The graphene monolayer is described by operators $c_{sk\sigma}^\dagger$ ($c_{sk\sigma}$) for creation (annihilation) of electrons in quantum states labeled by the wave number k , spin σ and valley index $s = 1, 2$. For the adatoms, $d_{j\sigma}^\dagger$ ($d_{j\sigma}$) creates (annihilates) an electron with spin σ with energy ε_{jd} , where $j = 1, 2$ correspond to the upper and lower adatoms, respectively. The third term in Eq.(1) accounts for the on-site Coulomb interaction \mathcal{U} , with $n_{d_j\sigma} = d_{j\sigma}^\dagger d_{j\sigma}$. Finally, the last term mixes the graphene and the levels ε_{jd} , wherein H.c. gives the Hermitian conjugate of the first part. This mixing is characterized by the coupling $\mathcal{V}_k = \frac{1}{2\pi} \sqrt{\frac{\pi\Omega_0}{\mathcal{N}}} \sqrt{|k|} v_0 (1 - q_0 \frac{\hbar v_F k}{D})$, where \mathcal{N} is the number of conduction states, Ω_0 denotes the unit cell area, and

$$q_0 = \frac{v_1 D}{v_0 t} \quad (2)$$

is the Fano factor of interference defined according to the results of Ref.[12]. The parameter t stands for the coupling strength between carbon atoms, while v_0 and v_1 represent the host-adatom hybridizations outlined in Fig.1 and $D = 7\text{eV}$ denotes the band-edge for $v_F \sim c/300$. The Fano factor q_0 can be tuned assisted by a variation of v_F , which enters into $t = \frac{2\hbar}{3a} v_F$ ¹³ and $\frac{v_1 D}{v_0}$. The experimental tuning of v_F can be achieved, for instance, by means of modifying the carrier concentration in suspended graphene¹⁴ [inset of Fig.1(a)].

The situation $q_0 = 0$ corresponds to the scenario in which collinear adatoms are locally side-coupled to a

single carbon atom (local coupling regime). Otherwise, $q_0 \neq 0$ denotes the hybridization of the adatoms with the three second neighbors of carbons as depicted in Fig.1 (non-local coupling).

To analyze the transport properties of the geometry we consider and look for the existence of the BICs, we should focus on the local density of states of the host (LDOS) and those corresponding for the adatoms (DOS). The former defines the conductance of the device at zero temperature $T = 0^+$:

$$G \sim \frac{e^2}{h} \Gamma_{\text{tip}} \text{LDOS}, \quad (3)$$

with $\Gamma_{\text{tip}} = \pi t_c^2 \rho_{\text{tip}}$, ρ_{tip} as the STM tip density of states.

To obtain the value of LDOS probed by the STM tip of Fig.1, we should consider the tunneling Hamiltonian

$$\mathcal{H}_{\text{tun}} = t_c \sum_{\sigma} \psi_{\text{tip},\sigma}^\dagger \Psi_{\sigma} + \text{H.c.}, \quad (4)$$

where $\psi_{\text{tip},\sigma}$ and Ψ_{σ} are respectively fermionic operators for the edge site of the STM tip and

$$\Psi_{\sigma} = \frac{1}{2\pi} \sqrt{\frac{\pi\Omega_0}{\mathcal{N}}} \sum_s \int \sqrt{|k|} (1 - q_0 \frac{\hbar v_F k}{D}) dk c_{sk\sigma} + \frac{t_{d_1}}{t_c} d_{1\sigma} \quad (5)$$

is the field operator accounting for the quantum state of the graphene site placed right beneath the tip with hopping terms (t_{d_1} and t_c), cf. Fig.1. LDOS then can be computed as

$$\text{LDOS} = -\frac{1}{\pi} \sum_{\sigma} \text{Im}[\tilde{\mathcal{G}}_{\sigma}(\varepsilon^+)] = 2\mathcal{D}_0 + \sum_{\sigma jl} \Delta \text{LDOS}_{jl\sigma}, \quad (6)$$

where $\tilde{\mathcal{G}}_{\sigma}(\varepsilon^+)$ is the time Fourier transform of the Green's function

$$\mathcal{G}_{\sigma} = -\frac{i}{\hbar} \theta(\tau) \text{Tr}\{\varrho_{2D}[\Psi_{\sigma}(\tau), \Psi_{\sigma}^\dagger(0)]_+\} \quad (7)$$

and

$$\mathcal{D}_0 = \frac{|\varepsilon|}{D^2} (1 - q_0 \frac{\varepsilon}{D})^2 \quad (8)$$

is the graphene DOS, $\Delta \text{LDOS}_{jl\sigma}$ stands for the part induced by the adatoms (see detailed derivation for it in the Appendix).

It is worth mentioning that $\Delta \text{LDOS}_{jl\sigma}$ for $j \neq l$ represents electronic waves of a given spin σ that travel forth and back between the upper and lower adatoms showed in Fig.1(a), which for a specific energy ε , become phase shifted by π (Fano dip) with respect to the waves scattered by the adatoms, which are described by $\Delta \text{LDOS}_{jj\sigma}$. As discussed in Ref.[1], such scattering process then provides a mechanism of the emergence of BICs. This effect can be captured in the detailed derivation of LDOS appearing in the Appendix.

According to the Appendix, the evaluation of $\Delta\text{LDOS}_{jl\sigma}$ depends on the Green's functions $\tilde{\mathcal{G}}_{d_{j\sigma}d_{l\sigma}}$ ($j = 1, 2$ and $l = 1, 2$) for the adatoms. Additionally, to perceive the BICs emergence in our system, we should know the density of states DOS_{jj}^σ of these adatoms, which are determined as follows:

$$\text{DOS}_{jj}^\sigma = -\frac{1}{\pi} \text{Im}(\tilde{\mathcal{G}}_{d_{j\sigma}d_{j\sigma}}). \quad (9)$$

Thus both $\Delta\text{LDOS}_{jl\sigma}$ and DOS_{jj}^σ can be found by employing the Hubbard I approach¹⁵ at $T = 0$, since the determined Hubbard bands match with those obtained via the Numerical Renormalization Group, in particular, for graphene with a single adatom¹⁶. As a result, we can safely extrapolate the Hubbard I method to our graphene system. We start employing the equation-of-motion method to a single particle retarded Green's function of an adatom in time domain $\mathcal{G}_{d_{l\sigma}d_{j\sigma}} = -\frac{i}{\hbar}\theta(\tau) \text{Tr}\{\rho_{2\text{D}}[d_{l\sigma}(\tau), d_{j\sigma}^\dagger(0)]_+\}$, where $\theta(\tau)$ is the Heaviside function, $\rho_{2\text{D}}$ is the density matrix of the system described by the Hamiltonian of Eq.(1) and $[\dots, \dots]_+$ is the anticommutator between operators taken in the Heisenberg picture. Performing elementary algebra one obtains in the energy domain:

$$(\varepsilon^+ - \varepsilon_{ld})\tilde{\mathcal{G}}_{d_{l\sigma}d_{j\sigma}} = \delta_{lj} + \Sigma \sum_{\bar{l}} \tilde{\mathcal{G}}_{d_{\bar{l}\sigma}d_{j\sigma}} + \mathcal{U}\tilde{\mathcal{G}}_{d_{l\sigma}n_{d_1\bar{\sigma}},d_{j\sigma}}, \quad (10)$$

where $\varepsilon^+ = \varepsilon + i0^+$ and

$$\Sigma = \sum_s \int dk \frac{\mathcal{V}_k \mathcal{V}_k}{\varepsilon^+ - \hbar v_F k} = -\frac{v_0^2}{D^2} \varepsilon (1 - q_0 \frac{\varepsilon}{D})^2 \ln \left| \frac{D^2 - \varepsilon^2}{\varepsilon^2} \right| + \frac{v_0^2}{D} q_0 (2 - q_0 \frac{\varepsilon}{D}) - i\Delta \quad (11)$$

is the self-energy. Its imaginary part Δ is proportional to the scattering rate of the quasiparticles and is known as pseudogap. The latter is proportional to the local density of states of the host \mathcal{D}_0 given by Eq.(8), i.e., $\Delta = \pi v_0^2 \mathcal{D}_0$ ^{8,9}. Thus

$$\Delta = \frac{\pi v_0^2}{D^2} |\varepsilon| (1 - q_0 \frac{\varepsilon}{D})^2, \quad (12)$$

which depending on the value of the Fano parameter, the main contribution to the pseudogap can be linear, cubic or quadratic. As we will see in the discussion section, the latter situation is of particular interest, since magnetic BICs are formed in this case.

In Eq.(10) $\tilde{\mathcal{G}}_{d_{l\sigma}n_{d_1\bar{\sigma}},d_{j\sigma}}$ is a two particle Green's function composed by four fermionic operators, obtained from the time Fourier transform of $\mathcal{G}_{d_{l\sigma}n_{d_1\bar{\sigma}},d_{j\sigma}} = -\frac{i}{\hbar}\theta(\tau) \text{Tr}\{\rho_{2\text{D}}[d_{l\sigma}(\tau) n_{d_1\bar{\sigma}}(\tau), d_{j\sigma}^\dagger(0)]_+\}$, with $n_{d_1\bar{\sigma}} = d_{l\bar{\sigma}}^\dagger d_{l\bar{\sigma}}$ and spin $\bar{\sigma}$ (opposite to σ). Thus we first calculate the time derivative of $\mathcal{G}_{d_{l\sigma}n_{d_1\bar{\sigma}},d_{j\sigma}}$ and then its time

Fourier transform, which leads to

$$(\varepsilon^+ - \varepsilon_{ld} - \mathcal{U})\tilde{\mathcal{G}}_{d_{l\sigma}n_{d_1\bar{\sigma}},d_{j\sigma}} = \delta_{lj} \langle n_{d_1\bar{\sigma}} \rangle + \sum_s \int dk \mathcal{V}_k (\tilde{\mathcal{G}}_{c_{sk\sigma}d_{l\bar{\sigma}}^\dagger d_{l\bar{\sigma}},d_{j\sigma}} - \tilde{\mathcal{G}}_{c_{sk\bar{\sigma}}^\dagger d_{l\bar{\sigma}} d_{l\sigma},d_{j\sigma}} + \tilde{\mathcal{G}}_{d_{l\bar{\sigma}}^\dagger c_{sk\bar{\sigma}} d_{l\sigma},d_{j\sigma}}), \quad (13)$$

expressed in terms of new Green's functions of the same order of $\tilde{\mathcal{G}}_{d_{l\sigma}n_{d_1\bar{\sigma}},d_{j\sigma}}$ and the occupation number $\langle n_{d_1\bar{\sigma}} \rangle$ determined by

$$\langle n_{d_1\bar{\sigma}} \rangle = -\frac{1}{\pi} \int_{-D}^{\varepsilon_F=0} \text{Im}(\tilde{\mathcal{G}}_{d_{1\bar{\sigma}}d_{1\bar{\sigma}}}) d\varepsilon. \quad (14)$$

We highlight that for the quadratic pseudogap, the self-consistent evaluation of the Eq.(14) reveals a range of magnetic solutions with $\langle n_{d_1\uparrow} \rangle \neq \langle n_{d_1\downarrow} \rangle$ for the values of q_0 , lying in the range between two critical points q_{c1} and q_{c2} . Outside the magnetic region, i.e., for different scalings of the pseudogap ($\Delta \propto |\varepsilon|, |\varepsilon|^2$ for $q_0 < q_{c1}$ and $\Delta \propto |\varepsilon|^3$ for $q_0 > q_{c2}$), Eq.(14) has non-magnetic solutions with $\langle n_{d_1\uparrow} \rangle = \langle n_{d_1\downarrow} \rangle$ only. This point will be addressed in detail in Sec.III of the paper (see in particular Fig.2).

Furthermore, by employing the Hubbard I approximation, we decouple the Green's functions in the right-hand side of Eq.(13) as performed in Ref.[1]. This procedure enables us to solve the system of Green's functions within Eq.(10), leading to $\tilde{\mathcal{G}}_{d_{j\sigma}d_{j\sigma}} = \frac{\lambda_j^\sigma}{\varepsilon - \varepsilon_{jd} - \Sigma_{jj}^\sigma}$, where $\lambda_j^\sigma = (1 + \frac{\mathcal{U}\langle n_{d_j\bar{\sigma}} \rangle}{\varepsilon - \varepsilon_{jd} - \mathcal{U} - \Sigma})$, and:

$$\tilde{\Sigma}_{jj}^\sigma = \Sigma + \lambda_j^\sigma \lambda_j^\sigma \frac{\Sigma^2}{\varepsilon - \varepsilon_{jd} - \Sigma} \quad (15)$$

is the total self-energy, with $\bar{j} = 2, 1$ respectively for $j = 1, 2$ in order to identify distinct adatoms and $\tilde{\mathcal{G}}_{d_{j\sigma}d_{j\sigma}} = \frac{\lambda_j^\sigma \Sigma \tilde{\mathcal{G}}_{d_{\bar{j}\sigma}d_{\bar{j}\sigma}}}{\varepsilon - \varepsilon_{jd} - \Sigma}$ are mixed Green's functions.

III. RESULTS AND DISCUSSION

In the simulations we adopt $T = 0$ and the set of parameters¹: $\varepsilon_{jd} = \varepsilon_d = -0.07D$, which is feasible in suspended graphene (inset of Fig.1(a))¹⁴ and $\mathcal{U} = v_0 = -2\varepsilon_d$. Additionally, to avoid that BICs decay into the continuum, we use $t_{d_1}/t_c = 0$, otherwise it leads to experimental detection of BICs by means of the so-called quasi-BICs¹.

In Fig.2 three distinct regions in the occupation numbers of Eq.(14) for $j = 1, 2$ appear identified by their corresponding pseudogaps Δ [Eq.(12)]: the non-magnetic regions corresponding to small or big Fano factors appear to be divided by a magnetic central domain delimited by the critical values q_{c1} and q_{c2} . At critical values, abrupt jumps in the occupation numbers point out the existence

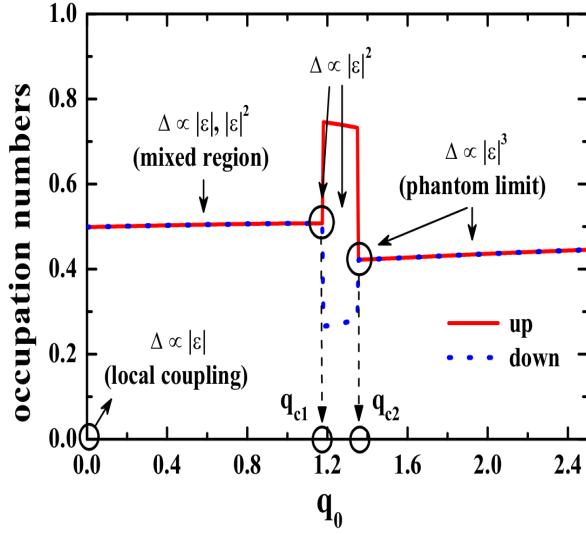


Figure 2. (Color online) Occupation numbers given by Eq.(14) for spin-up and spin-down states of the adatoms as a function of q_0 .

of a QPT connected with the spin degree of freedom. Panel (a) of Fig. 3 presents the DOS corresponding to the regime $q_0 = 0.8 < q_{c1}$ where one can clearly see resolved and spin-degenerate peaks in Eq. (9) for the DOS_{jj}^σ . In Fig. 3(b) spin-polarized peaks emerge when the Fano factor is placed within the boundaries $q_{c1} < q_0 = 1.2 < q_{c2}$, while in panel (c) the case of $q_0 = 2.0$ corresponds to the limit of the phantom atom considered in detail in Ref.[1] for which spin degeneracy is recovered.

To demonstrate that the system possesses BICs, we compare the density of states DOS_{jj}^σ for adatoms shown in Fig.3 with the host local density of states $\Delta LDOS_{jj\sigma}$ depicted at Fig.4. As one can see, both quantities reveal pronounced peaks (resonant states) placed at the same positions. Particularly in panels (a) and (b) of Fig. 4 with $q_0 = 0.8$, we observe as aftermath of Eq.(A.13), degenerate spin-up and down components for the Fano dips of $\Delta LDOS_{jl\sigma}$ ($l \neq j$) interfering destructively with the peaks found in $\Delta LDOS_{jj\sigma}$. As this interference is completely perfect, BICs emerge at the positions marked by vertical lines crossing panels (a), (b) and (c) of this figure. In panel (c) of the same figure, the total LDOS of Eq. (6) reveals absence of peaks at those places in which such a destructive interference occurs within panels (a) and (b). The aforementioned positions without peaks in Fig. 4(c) thereby give rise to BICs: the total LDOS that determines the conductance does not catch the same peaks found in Fig. 3(a) for the adatoms. Thus the aforementioned invisibility of such resonant states points out that electrons with opposite spins stay equally trapped within these adatoms when $q_0 < q_{c1}$ and the pseudogap scales as $\Delta \propto |\epsilon|, |\epsilon|^2$.

Panels (a), (b) and (c) of Fig. 5 correspond to the case $q_{c1} < q_0 = 1.2 < q_{c2}$ where magnetic solutions become possible, since the pseudogap is ruled by $\Delta \propto |\epsilon|^2$. The

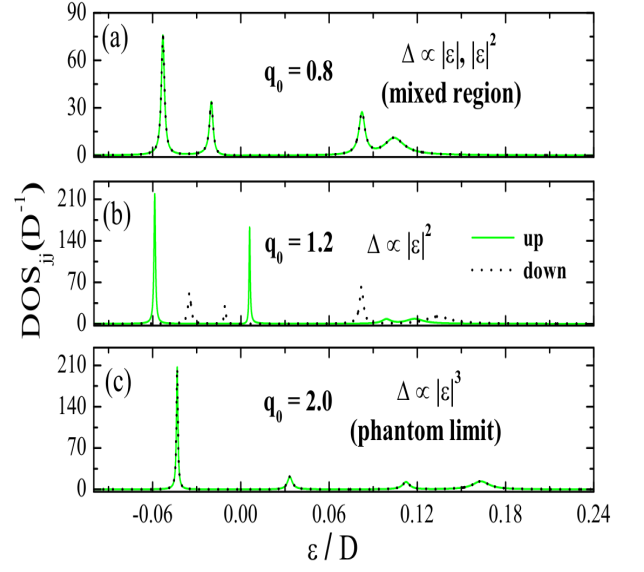


Figure 3. (Color online) (a) DOS for the case $q_0 < q_{c1}$. Well resolved spin degenerate peaks are clearly visible. (b) DOS for the case $q_{c1} < q_0 < q_{c2}$ with break of spin degeneracy. (c) DOS for the case $q_0 > q_{c2}$ when spin degeneracy is recovered.

position of magnetic BICs is denoted by vertical dashed lines. Consequently, in the domain $q_{c1} < q_0 < q_{c2}$, the novelty due to a non-local coupling between graphene and collinear adatoms lies on the possibility of tuning the spin of the electrons trapped in the BICs of the adatoms. Such a feature yields an emerging *based suspended graphene spintronics*, in which a spin-filter of BICs rises as a feasible application. Outside the critical domain, just spin-degenerate BICs exist.

Let us now present the physical arguments that elucidate the emergence of the reported magnetic BICs, which is indeed triggered by a QPT. Similar QPT appearing due to the quadratic scaling of the pseudogap $\Delta \propto |\epsilon|^2$ and related breaking of the spin-degeneracy was discussed in Ref. [8], where a double dot system was explored. In regard of this dot setup, we highlight that the pseudogap $\Delta \propto |\epsilon|^2$ is only revealed to be present after performing a mapping of the original Hamiltonian into an effective model, in particular, under restricted constraints. On the other hand, we demonstrate that graphene emerges as the natural platform wherein the pseudogap of Eq.(12) includes not only the regime $|\epsilon|^2$, but also $|\epsilon|, |\epsilon|^2$ and $|\epsilon|^3$, just due to the non-local adatom-graphene coupling. These regimes are accessible by means of the tuning of the Fano factor q_0 , which here is proposed to be practicable by developing the Fermi velocity engineering¹⁴. Moreover, the non-local coupling assumption improves the emulation of the experimental reality, since the standard case of local coupling regime, which is widely employed in the literature, is indeed ideal and hides completely the reported QPT.

Fig.6 illustrates how spin-resolved DOS of the adatoms

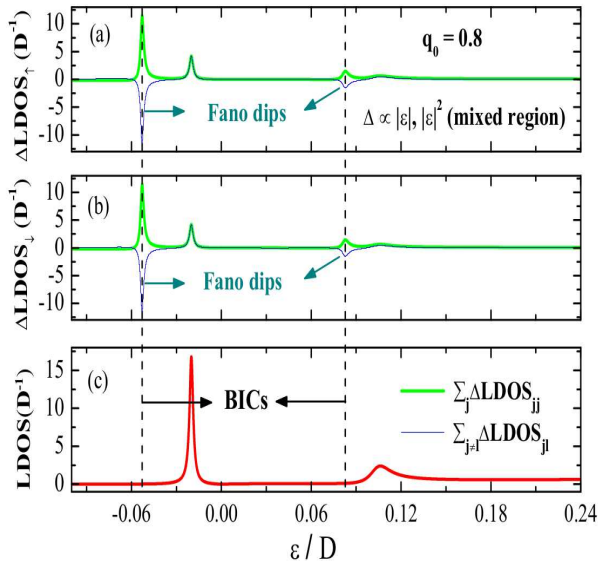


Figure 4. (Color online) Host local density of states corresponding to the cases of non-magnetic BICs (panels (a), (b), and (c)). BICs appear when a peak in $\Sigma_j \Delta \text{LDOS}_{jj\sigma}$ is fully compensated by a Fano dip in $\Sigma_{j \neq l} \Delta \text{LDOS}_{jl\sigma}$. Positions of BICs are marked by vertical dashed lines. Panels (a) and (b) correspond to spin resolved ΔLDOS . Lower panel (c) corresponds to total LDOS defining the conductance.

depend on the Fano parameter. The variation of q_0 in the wide range below the critical value $q_{c1} \approx 1.1766$ shifts the position of the peaks corresponding to opposite spin components equally, as it is shown in the upper panel. However, above the critical value the spin splitting abruptly appears as it is shown at the lower panel of the figure, which clearly indicates that the system undergoes a QPT. The abrupt appearance of the spin splitting is intimately connected with the step-like behavior observed in the occupation numbers shown in Fig. 2. Note that the increase of the Fano factor above the second critical value q_{c2} leads to the recovering of the spin-degeneracy as the regime of the phantom atom with cubic scaling of the pseudogap $\Delta \propto |\varepsilon|^3$ is achieved.

Within the critical boundaries $q_{c1} < q_0 < q_{c2}$, the quantity $\text{Re}(\tilde{\Sigma}_{jj}^{\sigma} - \Sigma) \equiv \mathcal{J}^{\text{exch}}$ from Eq.(15) plays the role of a Zeeman-like splitting of the levels ε_d in the adatoms. This splitting arises from an intrinsic exchange field $\mathcal{J}^{\text{exch}}$ between the adatoms intermediated by the graphene monolayer. Its value is ruled by the system natural control parameter, namely the Fano factor q_0 , which drives the graphene system towards a QPT. As the upper and lower adatoms magnetize equally, cf. Fig. 2, the coupling between them is revealed as ferromagnetic. Note that the dependence of the effective field on the Fano parameter is non-monotonous: it drops abruptly when $q_0 = q_{c2} \approx 1.3582$.

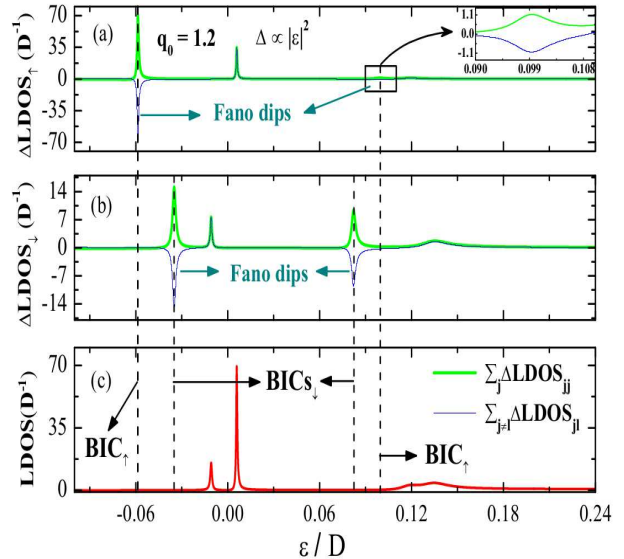


Figure 5. (Color online) Host local density of states corresponding to the cases of magnetic BICs (panels (a), (b), and (c)).

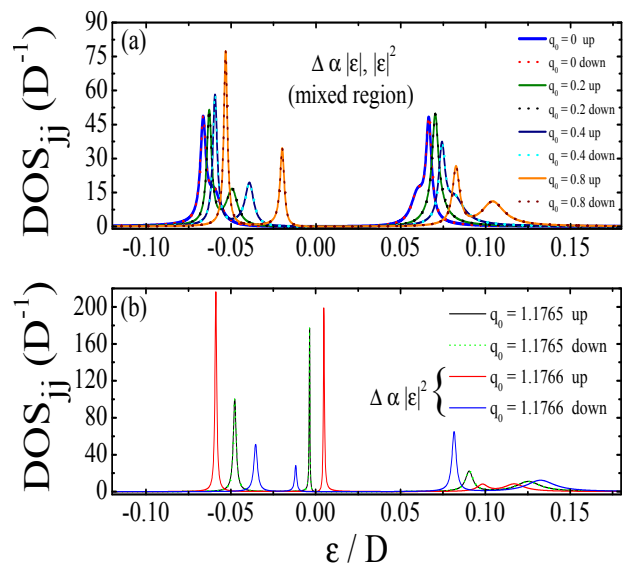


Figure 6. (Color online) (a) Spin-degenerate crossover from merged peaks of Eq.(9) for the adatoms DOS towards to resolved peaks. (b) QPT due to an abrupt spin-splitting of the peaks.

IV. CONCLUSIONS

In summary, we have proposed a setup based on graphene-adatom system in which magnetic BICs are triggered by a quantum phase transition in the region of the quadratic scaling of the pseudogap with energy, $\Delta \propto |\varepsilon|^2$. The control parameter which drives this transition is a Fano factor of interference tunable by changing the slope of the Dirac cones in graphene band-structure.

V. ACKNOWLEDGMENTS

This work was supported by CNPq, CAPES, 2014/14143-0 São Paulo Research Foundation (FAPESP), RISE project 644076 CoExAN, FP7 IRSES project QOCaN and Rannis project “Bose and Fermi systems for spintronics”. A. C. S. thanks the NTU at Singapore for hospitality.

Appendix: LDOS derivation

To obtain the analytical expressions of the LDOS given by Eq.(6) appearing in the conductance of Eq.(3), we begin by applying the equation-of-motion approach to $\mathcal{G}_\sigma = -\frac{i}{\hbar}\theta(\tau)\text{Tr}\{\varrho_{2D}[\Psi_\sigma(\tau), \Psi_\sigma^\dagger(0)]_+\}$, with Eq.(5) rewritten as

$$\begin{aligned} \Psi_\sigma &= \frac{1}{2\pi}\sqrt{\frac{\pi\Omega_0}{\mathcal{N}}}\sum_s\int\sqrt{|k|}\left(1-q_0\frac{\hbar v_F k}{D}\right)dkc_{sk\sigma} \\ &+ (\pi\mathcal{D}_0v_0)\sum_j\mathcal{C}_jd_{j\sigma}, \end{aligned} \quad (\text{A.1})$$

expressed in terms of $\mathcal{C}_j = (\pi\mathcal{D}_0v_0)^{-1}(t_{d_1}/t_c)\delta_{j1}$. Substituting Eq. (A.1) in \mathcal{G}_σ , one finds

$$\begin{aligned} \mathcal{G}_\sigma &= \left(\frac{1}{2\pi}\sqrt{\frac{\pi\Omega_0}{\mathcal{N}}}\right)^2\sum_{\bar{s}\bar{s}}\int\sqrt{|k|}\left(1-q_0\frac{\hbar v_F k}{D}\right)dk \\ &\times\sqrt{|q|}\left(1-q_0\frac{\hbar v_F q}{D}\right)dq\mathcal{G}_{c_{sk\sigma}c_{\bar{s}q\sigma}}+(\pi\mathcal{D}_0v_0)\sum_{j\bar{s}}\mathcal{C}_j \\ &\times\left(\frac{1}{2\pi}\sqrt{\frac{\pi\Omega_0}{\mathcal{N}}}\right)\int\sqrt{|k|}\left(1-q_0\frac{\hbar v_F k}{D}\right)dk \\ &\times(\mathcal{G}_{d_{j\sigma}c_{sk\sigma}}+\mathcal{G}_{c_{sk\sigma}d_{j\sigma}})+(\pi\mathcal{D}_0v_0)^2\sum_{jl}\mathcal{C}_j\mathcal{C}_l\mathcal{G}_{d_{j\sigma}d_{l\sigma}}, \end{aligned} \quad (\text{A.2})$$

with the new Green's functions $\mathcal{G}_{c_{sk\sigma}c_{\bar{s}q\sigma}}$, $\mathcal{G}_{d_{j\sigma}c_{sk\sigma}}$, $\mathcal{G}_{c_{sk\sigma}d_{j\sigma}}$ and $\mathcal{G}_{d_{j\sigma}d_{l\sigma}}$ to be determined. To this end, we first consider $\mathcal{G}_{c_{sk\sigma}c_{\bar{s}q\sigma}} = -\frac{i}{\hbar}\theta(\tau)\text{Tr}\{\varrho_{2D}[c_{sk\sigma}(\tau), c_{\bar{s}q\sigma}^\dagger(0)]_+\}$, whose time derivative $\partial_\tau \equiv \frac{\partial}{\partial\tau}$ gives

$$\begin{aligned} \partial_\tau\mathcal{G}_{c_{sk\sigma}c_{\bar{s}q\sigma}} &= -\frac{i}{\hbar}\delta(\tau)\text{Tr}\{\varrho_{2D}[c_{sk\sigma}(\tau), c_{\bar{s}q\sigma}^\dagger(0)]_+\} \\ &- \frac{i}{\hbar}(\hbar v_F k)\mathcal{G}_{c_{sk\sigma}c_{\bar{s}q\sigma}} - \frac{i}{\hbar}\sum_j\mathcal{V}_k\mathcal{G}_{d_{j\sigma}c_{\bar{s}q\sigma}}, \end{aligned} \quad (\text{A.3})$$

where we have used

$$\begin{aligned} i\hbar\partial_\tau c_{sk\sigma}(\tau) &= [c_{sk\sigma}, \mathcal{H}_{2D}] = (\hbar v_F k)c_{sk\sigma}(\tau) \\ &+ \sum_j\mathcal{V}_kd_{j\sigma}(\tau). \end{aligned} \quad (\text{A.4})$$

In the energy domain after performing the time Fourier transform, we solve Eq. (A.3) for $\tilde{\mathcal{G}}_{c_{sk\sigma}c_{\bar{s}q\sigma}}$ and obtain

$$\tilde{\mathcal{G}}_{c_{sk\sigma}c_{\bar{s}q\sigma}} = \frac{\delta(k-q)\delta_{\bar{s}\bar{s}}}{\varepsilon^+ - \hbar v_F k} + \sum_j\frac{\mathcal{V}_k}{\varepsilon^+ - \hbar v_F k}\tilde{\mathcal{G}}_{d_{j\sigma}c_{\bar{s}q\sigma}}. \quad (\text{A.5})$$

Notice that we also need to calculate the mixed Green's function $\tilde{\mathcal{G}}_{d_{j\sigma}c_{\bar{s}q\sigma}}$. We then define the advanced Green's function $\mathcal{F}_{d_{j\sigma}c_{\bar{s}q\sigma}} = \frac{i}{\hbar}\theta(-\tau)\text{Tr}\{\varrho_{2D}[d_{j\sigma}^\dagger(0), c_{\bar{s}q\sigma}(\tau)]_+\}$, whose equation-of-motion reads,

$$\begin{aligned} \partial_\tau\mathcal{F}_{d_{j\sigma}c_{\bar{s}q\sigma}} &= -\frac{i}{\hbar}\delta(\tau)\text{Tr}\{\varrho_{2D}[d_{j\sigma}^\dagger(0), c_{\bar{s}q\sigma}(\tau)]_+\} \\ &- \frac{i}{\hbar}(\hbar v_F q)\mathcal{F}_{d_{j\sigma}c_{\bar{s}q\sigma}} - \frac{i}{\hbar}\sum_l\mathcal{V}_q\mathcal{F}_{d_{j\sigma}d_{l\sigma}}, \end{aligned} \quad (\text{A.6})$$

where we have used once again Eq. (A.4), interchanging $k \leftrightarrow q$. The Fourier transform of Eq. (A.6) leads to

$$\varepsilon^-\tilde{\mathcal{F}}_{d_{j\sigma}c_{\bar{s}q\sigma}} = (\hbar v_F q)\tilde{\mathcal{F}}_{d_{j\sigma}c_{\bar{s}q\sigma}} + \sum_l\mathcal{V}_q\tilde{\mathcal{F}}_{d_{j\sigma}d_{l\sigma}}, \quad (\text{A.7})$$

with $\varepsilon^- = \varepsilon - i0^+$. Applying the property $\tilde{\mathcal{G}}_{d_{j\sigma}c_{\bar{s}q\sigma}} = (\tilde{\mathcal{F}}_{d_{j\sigma}c_{\bar{s}q\sigma}})^\dagger$ on Eq. (A.7), we show that

$$\varepsilon^+\tilde{\mathcal{G}}_{d_{j\sigma}c_{\bar{s}q\sigma}} = (\hbar v_F q)\tilde{\mathcal{G}}_{d_{j\sigma}c_{\bar{s}q\sigma}} + \sum_l\mathcal{V}_q\tilde{\mathcal{G}}_{d_{j\sigma}d_{l\sigma}}, \quad (\text{A.8})$$

$$\tilde{\mathcal{G}}_{d_{j\sigma}c_{\bar{s}q\sigma}} = \sum_l\frac{\mathcal{V}_q}{\varepsilon^+ - \hbar v_F q}\tilde{\mathcal{G}}_{d_{j\sigma}d_{l\sigma}} \quad (\text{A.9})$$

and analogously,

$$\tilde{\mathcal{G}}_{c_{sk\sigma}d_{j\sigma}} = \sum_l\frac{\mathcal{V}_q}{\varepsilon^+ - \hbar v_F q}\tilde{\mathcal{G}}_{d_{l\sigma}d_{j\sigma}}. \quad (\text{A.10})$$

Now we substitute Eq. (A.9) into Eq. (A.5) and the latter, together with Eqs. (A.10) and (11) for the self-energy splitted as

$$\Sigma = \sum_s\int dk\frac{\mathcal{V}_k\mathcal{V}_k}{\varepsilon^+ - \hbar v_F k} = \pi v_0^2\mathcal{D}_0(\tilde{\mathcal{A}}_j - i\mathcal{B}_j), \quad (\text{A.11})$$

into Eq. (A.2) in the energy domain, which results in

$$\begin{aligned} \tilde{\mathcal{G}}_\sigma &= \left(\frac{1}{2\pi}\sqrt{\frac{\pi\Omega_0}{\mathcal{N}}}\right)^2\sum_s\int(1-q_0\frac{\hbar v_F k}{D})^2kdk\frac{1}{\varepsilon^+ - \varepsilon_k} \\ &+ (\pi\mathcal{D}_0v_0)^2\sum_{jl}(\tilde{\mathcal{A}}_j - i\mathcal{B}_j)\tilde{\mathcal{G}}_{d_{j\sigma}d_{l\sigma}}(\tilde{\mathcal{A}}_l - i\mathcal{B}_l) \\ &+ (\pi\mathcal{D}_0v_0)^2\sum_{jl}\mathcal{C}_j(\tilde{\mathcal{A}}_l - i\mathcal{B}_l)(\tilde{\mathcal{G}}_{d_{j\sigma}d_{l\sigma}} + \tilde{\mathcal{G}}_{d_{l\sigma}d_{j\sigma}}) \\ &+ (\pi\mathcal{D}_0v_0)^2\sum_{jl}\mathcal{C}_j\mathcal{C}_l\tilde{\mathcal{G}}_{d_{j\sigma}d_{l\sigma}}. \end{aligned} \quad (\text{A.12})$$

Thus after some algebra via the evaluation of $-\frac{1}{\pi} \sum_{\sigma} \text{Im}(\tilde{\mathcal{G}}_{\sigma})$, we determine Eq.(6) as the LDOS probed by the STM tip, with

$$\Delta\text{LDOS}_{jl\sigma} = -(\pi v_0^2 \mathcal{D}_0^2) \text{Im}[(\mathcal{A}_l - i\mathcal{B}_l) \tilde{\mathcal{G}}_{d_{l\sigma} d_{j\sigma}} (\mathcal{A}_j - i\mathcal{B}_j)], \quad (\text{A.13})$$

$$\text{with } \mathcal{A}_j = \frac{1}{\pi v_0^2 \mathcal{D}_0} \text{Re}\Sigma + \delta_{j1} (\pi^2 v_0^2 \mathcal{D}_0^2)^{-1/2} (t_{d1}/t_c) \text{ and } \mathcal{B}_j = -\frac{1}{\pi v_0^2 \mathcal{D}_0} \text{Im}\Sigma.$$

* Current address: Institute of Semiconductor and Solid State Physics, Johannes Kepler University Linz, Austria.

¹ L.H. Guessi *et al.*, Phys. Rev. B **92**, 045409 (2015).

² W.-J. Gong *et al.*, Nanoscale Res. Lett. **8**, 330 (2013).

³ J. von Neumann and E. Wigner, Phys. Z. **30**, 465 (1929).

⁴ F.H. Stillinger and D.R. Herrick, Phys. Rev. A **11**, 446 (1975).

⁵ Y. Boretz *et al.*, Phys. Rev. A **90**, 023853 (2014).

⁶ A. Crespi *et al.*, Phys. Rev. Lett. **114**, 090201 (2015).

⁷ U. Fano, Phys. Rev. **124**, 1866 (1961).

⁸ L.G.G. V. Dias da Silva *et al.*, Phys. Rev. Lett. **97**, 096603 (2006).

⁹ C.G.-Buxton and K. Ingersent, Phys. Rev. B **57**, 14254 (1998).

¹⁰ P.W. Anderson, Phys. Rev. **124**, 41 (1961).

¹¹ Z.-G. Zhu, K.-H. Ding, and J. Berakdar, Europhys. Lett. **90**, 67001 (2010).

¹² A.C. Seridonio, M. Yoshida, and L.N. Oliveira, Europhys. Lett. **86**, 67006 (2009).

¹³ A.H. Castro Neto *et al.*, Rev. Mod. Phys. **81**, 109 (2009).

¹⁴ D.C. Elias *et al.*, Nat. Phys. **7**, 701 (2011).

¹⁵ J. Hubbard, Proc. R. Soc. Lond. A, **281**, 401 (1964).

¹⁶ P.S. Cornaglia, G. Usaj, and C.A. Balseiro, Phys.Rev. Lett. **102**, 046801 (2009).